The modelled climatic response to the 18.6-year lunar nodal cycle and its role in decadal temperature trends

Manoj Joshi[1,2], Robert A. Hall[1], David P. Stevens[3], Ed Hawkins[4]

5 [1]School of Environmental Sciences, University of East Anglia, Norwich NR4 7SQ, United Kingdom

[2]Climatic Research Unit, University of East Anglia, Norwich NR4 7SQ, United Kingdom

[3]School of Mathematics, University of East Anglia, Norwich NR4 7SQ, United kingdom

[4]National Centre for Atmospheric Science, Department of Meteorology, University of Reading, Reading RG6 6BB, United Kingdom

10 *Correspondence to:* Manoj Joshi (m.joshi@uea.ac.uk)

Abstract. The 18.6-year lunar nodal cycle arises from variations in the angle of the Moon's orbital plane. Previous work has linked the nodal cycle to climate but has been limited, either by the length of observations analysed, or geographical regions

15 considered in model simulations of the pre-industrial period. Here we examine the global effect of the lunar nodal cycle in multi-centennial climate model simulations of the pre-industrial period. We find cyclic signals in global and regional surface air temperature having amplitudes of O (0.1 K), ocean heat uptake and ocean heat content. The timing of anomalies of global surface air temperature and heat uptake are consistent with the so-called slowdown in global warming in the first decade of the 21st century, also displaying warmer than average Arctic surface temperatures at the same time. The lunar nodal cycle

20 causes variations in mean sea level pressure exceeding 0.5 hPa in the Nordic seas region, thus affecting the North Atlantic Oscillation Index during boreal winter. Our results suggest that the contribution of the lunar nodal cycle to global temperature should be negative in the mid-2020s before becoming positive again in the early-2030s, reducing the uncertainty in time at which projected global temperature reaches 1.5C above pre-industrial levels.

25 **1. Introduction**

The lunar nodal cycle arises from variations in the angle of the Moon's orbital plane relative to plane of the Earth's equator (lunar declination), between 18.3° and 28.6°, over a period of 18.6 years (Pugh et al. 1987). A potential connection of this cycle to climate is through the modulation of ocean tides (Loder and Garrett 1978), the dissipation of which are a major driver of vertical diffusivity in the world's oceans (Pease et al. 1995). The change in lunar declination results in an 18.6-year period

30 modulation of all lunar and luni-solar tidal constituents, and potentially the resulting tidally-driven diffusivity. The amplitude of the modulation varies depending on tidal constituent, but for the dominant semidiurnal and diurnal constituents (M_2 and K_1) the modulation is small (3.7% and 11.5% respectively). Previous research has attempted to identify the effect of this signal in climate observations, but since the total modulation of the tide is small, demonstrating a significant effect on global temperature is extremely hard (Ray 2007). Regional climatic records, such as sea level in regions with large tides, or multi-century proxies,

35 have been shown to exhibit an 18.6 year cycle (Currie et al. 1984, Ynestad et al. 2006, Yasuda et al. 2006, Gratiot et al. 2008, Agosta et al. 2013, Hamamoto and Yasuda 2021).

Modelling studies of this phenomenon are relatively rare: simple studies considering modulated stratification in the ocean have suggested an effect on global temperature (Loder and Garrett 1978). More complex studies, involving ocean circulation models (Osafune and Yasuda 2013), and most recently coupled ocean-atmosphere models, have demonstrated an effect of the nodal

40 cycle on the circulation of the Pacific Ocean (Osafune et al. 2020), and suggested a link to variability in the Pacific basin, particularly the Pacific Decadal Oscillation (PDO) (Tanaka et al. 2012, Osafune et al. 2014).

Here we perform millennial length runs of a coupled ocean-atmosphere global circulation model (OAGCM) in order to quantify the effect of a parameterisation of the lunar nodal cycle on climate. The flexibility of the parameterisation allows for sensitivity tests to be conducted. We investigate the effect of the lunar nodal cycle on long-term trends, with a particular view

45 to understanding its role on the so-called 'slowdown' on global warming in the early part of the 21st century.

2. Method

Our research employs the FORTE2 climate model (Blaker et al. 2020), which uses the primitive equations of meteorology and oceanography on a sphere. The atmospheric component is the IGCM4, the ocean component is MOMA (Joshi et al. 2015,

50 Webb 1996). The IGCM4 is run in its full 35-layer stratosphere-resolving configuration, with a horizontal resolution approximating to 2.8°. MOMA is run with a 2° horizontal resolution, and 15 vertical levels. The background vertical diffusivity in the ocean component of the model, a large part of which is accounted for by tidal dissipation, is then modulated using a simple parameterisation that assumes all tidal energy is dissipated locally.

The nodal cycle parameterisation is constructed using the geographical distribution of RMS (root mean square) current velocity

55 magnitude for the 8 largest tidal constituents (M_2, S_2, N_2, K_2, K_1, O_1, P_1 and M_f), calculated from the TPXO7.2 inverse model (Egbert and Erofeeva 2002), multiplied by their nodal amplitudes (Pugh 1987) (e.g., −0.037 for M_2). The constituent-sum of modulated RMS velocity magnitude is divided by the constituent-sum of un-modulated RMS velocity magnitude, giving the relative modulation of tidal currents at each ocean gridpoint; such a normalisation is necessary because the parameterised tide in FORTE2, as in most OAGCMs, has constant amplitude in space. Note that modulations of M_2 and N_2 are 180° out of phase

60 with the other tidal constituents, so in regions with a strongly semidiurnal tidal regime (e.g., around New Zealand) the amplitude of the nodal cycle parameterisation may be negative. S_2 and P_1 are pure solar tides so are not directly modulated by the nodal cycle, however they do contribute to total un-modulated RMS velocity magnitude and so affect the relative modulation of tidal currents. The phase of the modulation is such that, at most grid points, tidal currents are maximum at 4.75 years into the cycle (e.g., June 2006).

65 The geographical shape of the function, determined by the relative strength of each tidal constituent at a given location and the constituent modulation amplitude, is shown in Figure 1: the Pacific and Arctic Oceans feature modulations of approximately 5% in amplitude, while the Atlantic Ocean has comparatively little modulation of tidally-driven diffusivity (typically <2%). Interestingly, the Arctic Ocean and Southern Ocean have large amplitudes in excess of 10% in places, indicating that climate may be significantly modulated by the nodal cycle in both regions. However, the water column is weakly stratified at high

70 latitudes, suggesting that the effect of tidal modulation in this region might actually be small.

Tides are known to play a controlling role in the energetics of the global ocean, dissipating well over half of the kinetic energy in the oceans, with the greatest dissipation occurring near the ocean floor (Munk and Wunsch 1998, Egbert and Ray 2000, St. Laurent et al. 2002). Accordingly, two perturbation runs have been performed, one in which the nodal cycle parameterisation is applied uniformly with depth to the vertical diffusivity ("Constant"), and one in which it is applied such that its amplitude

75 linearly decreases from 1 at a depth of 5000 m to 0 at the ocean surface ("Scaled"), to mirror the effect of tidal dissipation. The SCALED run should be seen as an underestimate of the near-surface effects of the lunar nodal cycle, with the CONSTANT run being an overestimate.

The nodal cycle modulation is applied with a period of 19 FORTE2 years. Given the length of the year in FORTE2 is 360 days, such an approximation results in a nodal cycle whose length in days is within 0.7% of the observed cycle. FORTE2 is 80 run for 2300 years, with years 1520-2280 being analysed, i.e. 760 years or 40 full cycles.

3. Results

The global averaged ocean temperature stratification has warm waters in the upper ocean and cooler waters at depth. As the amplitude of the tidally driven diffusion increases in the first phase of the nodal cycle, the global mean vertical temperature 85 gradient is reduced with surface waters cooling and deeper waters warming. The surface temperature anomalies are larger than those at depth, as the vertical temperature gradient is largest in the upper ocean, through the permanent thermocline. Figure 2 shows the evolution of 19-year global ocean temperature anomalies with depth as a function of the amplitude of the lunar nodal cycle diffusion modulation. In both SCALED and CONSTANT cases, the top 100-150 m of ocean displays a cooling (warming) in phase with maximum (minimum) vertical diffusion. In the absence of any feedback from the atmosphere, the 90 global mean sea surface temperature cold anomaly would be expected to peak half-way through the nodal cycle. However, the atmosphere almost immediately responds to the anomalously cool sea surface temperatures by fluxing heat into the ocean (Figure 3), causing an increase in total ocean heat content (Figure 3). The uptake of heat by the ocean results in a global ocean heat content anomaly approximately in quadrature with the surface heat flux and nodal cycle (Figure 2). The deeper (below approximately 1000 m) temperature anomalies are largely isolated from the surface forcing and are approximately in 95 quadrature with the nodal cycle (Figure 2). Thus the deep ocean response to the nodal cycle actually lags the response at the surface (see later). As the tidally driven diffusion reduces in the second half of the cycle, the situation described above is reversed.

Figure 4 shows the effect of the lunar nodal cycle on the model global mean surface temperature T_g expressed as a function of the phase of the cycle. A best fit of a 19-year harmonic to T_g shows the phases at which minimum and maximum cooling 100 occur. Minimum global temperatures are reached within a year of the maximum diffusion occurring at year 4.5: such behaviour should be contrasted with the modelled response to transient solar or volcanic forcing, where a lag of approximately 2-3 years is present between maximum forcing and response (vol/sol refs here). The amplitude of response in SCALED is 0.03±0.02 K while the amplitude of the response in CONSTANT is 0.06±0.02 K. The response in the SCALED run is statistically significant only at times of max/min T_g, while the larger response in the CONSTANT run is significant at more times. Figure 4 (bottom 105 panel) shows the response in the Arctic region. Here the pattern is very noisy, but there is some indication of a shift in phase of temperature, which is examined in more detail later.

We now analyse the geographically varying response of FORTE2 to the lunar nodal cycle. Figures 5 and 6 show the amplitude, and phase at which minimum T_{surf} is reached, respectively, for each model grid point. Most areas display minimum T_{surf} at years 3-6, consistent with Figure 4. The response in the CONSTANT run is larger and statistically significant in more areas 110 than the SCALED run. Notable feature of Figures 5 and 6 though are the large responses in the Northwest Pacific Ocean, consistent with previous work (Tanaka et al. 2012), and Nordic Seas. The fitted response is inconsistent with the relatively small tidal forcing in the Nordic seas (see Figure 1). In addition, both SCALED and CONSTANT runs show that minimum T_{surf} occurs in years 14-18, completely out of phase with the global response. This polar response can be understood in terms of the local stratification. In the Nordic Seas and Southern Ocean, the ocean temperature maximum occurs at mid-depth rather 115 than at the surface because salinity is the dominant stratifying property. As the internal ocean heat flux is upwards above the temperature maximum, increased (reduced) vertical diffusivity associated with the nodal cycle leads to higher (lower) surface temperatures.

The geographically varying phases suggest a potential for geographically varying temperature and circulation responses. Figures 7 and 8 show the amplitude and phase at which minimum MSLP is reached in northern winter season NDJFM

120   (November-March, respectively, for each model grid point. In most regions there is no significant response. In the Atlantic/European region, a significant signal does exist in both SCALED and CONSTANT runs, suggesting a minimum in MSLP of 0.5 hPa over NW Europe in years 16-21 (or years -3 to 2), indicating that the lunar nodal cycle may force a small negative anomaly of the North Atlantic Oscillation (NAO) at this time. There is some indication of a dipole across the Pacific Ocean, suggesting an El Niño Southern Oscillation (ENSO) response, which has been associated with the lunar nodal cycle

125   (Loder and Garrett 1978, Yasuda 2018), but the response is not statistically significant. A similar statistically insignificant result is found for the time-variation of the Atlantic Meridional Circulation (AMOC). We have analysed surface temperatures in the Nino 3.4 region but find no significant signal.

The long-term effects of the lunar nodal cycle are now examined, since the effect of the ocean circulation would be expected to 'redden' a 19-year periodic forcing signal into lower frequencies, measurable on longer timescales. Figure 9 shows decadal

130   T_{surf} anomalies in each run. There is an increase in the standard deviation of running decadal-mean temperature in the CONSTANT run, but no clear increase in the SCALED run. The presence of the lunar nodal cycle will add a small positive or negative tendency to warming decadal trends in the 21st century, as illustrated in Figure 10, which shows assessed trends (Lee et al. 2021) from the 6th Assessment Report of the Intergovernmental Panel on Climate Change (IPCC AR6). The lunar nodal cycle (bottom panel) is expected to act as a slight cooling influence on the climate in the mid 2020s, delaying the arrival of the

135   1.5C temperature threshold in SSPs with higher carbon emissions (shown in red), but is a warming influence in the early-mid 2030s, hastening the arrival of the 1.5C temperature threshold in SSPs with lower carbon emissions (shown in blue). The net effect is to reduce the spread in time at which the world is projected to reach 1.5C above pre-industrial levels from 5 years to 3 years.

140   **4. Discussion and Conclusions**

The timing of the lunar nodal cycle is of special interest when considering so-called hiatus and surge decades. A purported 'slowdown' of global temperatures at the start of the 21st century has been much discussed with mechanisms such as volcanic aerosol forcing (Santer et al. 2014) and stratospheric water vapour (Solomon et al. 2010) invoked as part of the explanation, although updated observational datasets show less of global temperature slowdown than previously identified (e.g. HadCRUT5

145   and others). Anomalously high heat uptake by the world's oceans (Meehl et al. 2011, Guemas et al. 2013) and circulation changes in the Pacific Ocean (Kosaka and Xie 2013) are also suggested. Figures 1 and 2 suggest a potential role for the lunar nodal cycle in driving decadal variations in warming rates, with the SCALED run implying an average flux of ~0.07+/-0.07 Wm^{-2} into the world's oceans over the period 2002-2011. While the uncertainty in the value is clearly large, its magnitude suggests that it cannot be discounted as an important driver of multidecadal variability of global temperature, given that the

150   additional heat uptake into the oceans during hiatus-type periods can be as little as 0.08 Wm^{-2} (Hedemann et al. 2017).

Our results suggest that the contribution of the lunar nodal cycle should be to give an average flux of ~0.07+/-0.07 Wm^{-2} into the world's oceans over the period 2020-2029, and vice versa in the period 2030-2039. Accordingly, its contribution to global temperature should be negative in the early 2020s before becoming positive again, with an amplitude of ~0.04 C. Given the magnitude of such changes, and the results shown in Figure 10, we suggest that a parameterisation of the lunar nodal cycle

155   should be implemented in 1D integrated assessment models (IAMs) in order that they better represent the effect of this repeatable and predictable source of climate variability on the impacts of climate change. Although it is known that inclusion of the cycle affects projections of future regional sea-level change, for example in the North Sea (Baart et al 2012), we find that the global modulation of global sea level is 1-2 mm (not shown), because of counteracting influences of hot and cold

anomalies in the ocean (Figure 2). Such a value is far less than the currently observed global sea rise of 3 mm yr^{-1} (Dangendorf
160 et al. 2019), suggesting that the impact of the lunar nodal cycle on global sea level rise is small.

The geographical nature of the response to the lunar nodal cycle is complex, with the Arctic response being almost in antiphase
with the rest of the world, reflecting the reversed temperature gradient in the upper ocean, i.e. the lack of a permanent stratifying
thermocline. Interestingly, maximum Arctic temperatures are modelled as occurring in years 5-9 of the cycle, or 2007-2011,
consistent with enhanced Arctic warming during this time (Stroeve et al. 2012). All other things being equal, similar warm
165 Arctic anomalies might be expected during 2026-2030. Figure 7 also implies that the NAO is likely to be more negative than
average at the same time.

A caveat in this work lies in the nature of the tracer vertical diffusion scheme which is being modulated. Here we use a simple
profile that represents the sum of all diffusion processes that has been tuned to give a good representation of the global
thermocline structure. State-of-the-art coupled climate models use a variety of more sophisticated vertical diffusion
170 parameterisations in combination to represent a number of different processes, including wind mixing, tidal mixing, and
internal gravity wave scattering (see Mackinnon et al. 2017). Only the tidal and internal tidal induced diffusion is enhanced by
the lunar nodal cycle. Thus, if this accounts for one half of the mixing that we apply (a conservative estimate) then we would
expect the magnitude of the response to be halved.

We have implemented a simple, flexible parameterisation of the lunar nodal cycle into an OAGCM, examined its effects on
175 multicentennial-length runs, and have assessed its potential effects on 21st century climate. Our results lend further weight to
the idea that the phenomenon should be parameterised in decadal-scale forecasts made using global circulation models (e.g.
Osafune et al 2014), as well as in integrated assessment models, given the potential effect of the lunar nodal cycle on future
climatic trends.

180 **Author Contribution**

MJ conceived the original idea and performed model runs. All authors contributed to analysis of results and writing.

Competing Interests

The authors declare that they have no conflict of interest

185

Data Availability

Lunar nodal cycle forcing data available at:

https://research-portal.uea.ac.uk/en/datasets/lunar-nodal-cycle-amplitude-modulation-map

190 **Acknowledgements**

The research presented in this paper was carried out on the High Performance Computing Cluster supported by the Research
and Specialist Computing Support service at the University of East Anglia. MJ acknowledges the support of NERC project
NE/N006348/1 (SMURPHS). We acknowledge useful discussions with Mark Prosser.

195

References

Agosta, E. A.: The 18.6-year nodal tidal cycle and the bi-decadal precipitation oscillation over the plains to the east of subtropical Andes, South America, Int. J. Climatol., 33, DOI: 10.1002/joc.3787, 2013.

Baart, F., van Gelder, P. H. A. J. M., de Ronde, J., van Konginsveld, M. and Wouters C.: The Effect of the 18.6-Year Lunar
200   Nodal Cycle on Regional Sea-Level Rise Estimates, J. Coast. Res., 28, 511-516, 2012.

Currie, R.: Evidence for 18.6-year lunar nodal drought in western North America during the past millennium, J. Geophys. Res., 89, 1247–1476, 1984.

Dangendorf, S., Hay, C., Calafat, F.M., Marcos, M., Piecuch, C. G., Berk, K. and Jensen, J.: Persistent acceleration in global sea-level rise since the 1960s. Nat. Clim. Chang. 9, 705–710, 2019.

205   Egbert, G. D., and Erofeeva, S. Y.: Efficient inverse modeling of barotropic ocean tides. J. Atmos. Oceanic Technol., 19, 183–204, 2002.

Egbert, G. D., and Ray, R. D.: Significant dissipation of tidal energy in the deep ocean inferred from satellite altimeter data. Nature, 405, 775-778, 2000.

Gratiot, N., Anthony, E. J., Gardel, A., Gaucherel, C., Priosy, C. and Wells, J. T.: Significant contribution of the 18.6 year
210   tidal cycle to regional coastal changes, Nature Geos., 1, 169-172, 2008.

Guemas, V., Doblas-Reyes, F. J., Andreu-Burillo, I. and Asif, M.: Retrospective prediction of the global warming slowdown in the past decade. Nature Climate Change., 3, 649–653, 2013.

Hamamoto, M. and Yasuda I.: Synchronized interdecadal variations behind regime shifts in the Pacific Decadal Oscillation, J. Oceanogr, 77, 383–392, 2021.

215   Hedemann, C., Mauritsen, T., Jungclaus J. and Marotzke J.: The subtle origins of surface-warming hiatuses, Nature Climate Change, 7, 336-339, 2017.

Joshi, M. M., Stringer, M., van der Wiel, K., O'Callaghan, A., and Fueglistaler, S.: IGCM4: a fast, parallel and flexible inter-mediate climate model, Geosci. Model Dev., 8, 1157–1167, 2015.

Kosaka, Y and Xie, S-P.: Recent global-warming hiatus tied to equatorial Pacific surface cooling. Nature, 501, 403–407,
220   2013.

Lee, J.-Y., Marotzke, J., Bala, G., Cao, L., Corti, S., Dunne, J. P., Engelbrecht, F., Fischer, E., Fyfe, J. C., Jones, C., Maycock, A., Mutemi, J., Ndiaye, O., Panickal, S., and Zhou, T., Future Global Climate: Scenario-Based Projections and Near-Term Information. In Climate Change 2021: The Physical Science Basis. Contribution of Working Group I to the Sixth Assessment Report of the Intergovernmental Panel on Climate Change [Masson-Delmotte, V., P. Zhai, A. Pirani, S.L.
225   Connors, C. Péan, S. Berger, N. Caud, Y. Chen, L. Goldfarb, M.I. Gomis, M. Huang, K. Leitzell, E. Lonnoy, J.B.R. Matthews, T.K. Maycock, T. Waterfield, O. Yelekçi, R. Yu, and B. Zhou (eds.)]. Cambridge University Press. In Press 2021.

Loder, J. W. and Garrett, C.: The 18.6-Year Cycle of Sea Surface Temperature in Shallow Seas, J. Geophys. Res., 83, 1967-1970, 1978.

MacKinnon, J. A., Alford, M. H., Ansong, J. K., Arbic, B. K., Barna, A., Briegleb, B. P., Bryan, F. O., Buijsman, M.
230   C., Chassignet, E. P., Danabasoglu, G., MacKinnon, J. A., Alford, M. H., Ansong, J. K., Arbic, B. K., Barna, A., Briegleb, B. P., Bryan, F. O., Buijsman, M. C., Chassignet, E. P., Danabasoglu, G., Diggs, S., Griffies, S. M., Hallberg, R. W., Jayne, S. R., Jochum, M., Klymak, J. M., Kunze, E., Large, W. G., Legg, S., Mater, B., Melet, A. V., Merchant, L. M., Musgrave, R., Nash, J. D., Norton, N. J., Pickering, A., Pinkel, R., Polzin, K., Simmons, H. L., Laurent, L. S. C., Sun, O. M., Trossman,

235 D. S., Waterhouse, A. F., Whalen, C. B., and Zhao, Z.: Climate process team on internal-wave driven ocean mixing. Bull.
Amer. Meteor. Soc., 98, 2429– 2454, 2017.

Meehl, G. A., Arblaster, J. M., Fasullo, J. Y., Hu, A. and Trenberth, K. E.: Model-based evidence of deep-ocean heat uptake
during surface-temperature hiatus periods. Nature Climate Change 1, 360–364, 2011.

Munk, W., and Wunsch, C.: Abyssal recipies II: energetics of tidal and wind mixing. Deep-Sea Res. I, 45, 1977-2010, 1998.

Osafune, S. and Yasuda, I.: Remote impacts of the 18.6 year period modulation of localized tidal mixing in the North
240 Pacific, J. Geophys. Res.,118, 3128-3137, 2013.

Osafune, S., Masuda, S. and Sugiura, N.: Role of the oceanic bridge in linking the 18.6 year modulation of tidal mixing and
long-term SST change in the North Pacific, Geophys. Res. Lett., 41, 7284– 7290, 2014.

Osafune, S., Kouketsu, S., Masuda, S. and Sugiura, N.: Dynamical ocean response controlling the eastward movement of a
heat content anomaly caused by the 18.6-year modulation of localized tidally induced mixing, J. Geophys. Res. Oceans, 125,
245 e2019JC015513, 2020.

Pease, C. H., Turet, P. and Pritchard, R. S.: Barents Sea tidal and inertial motions from Argos ice buoys during the
Coordinated Eastern Arctic Experiment. J. Geophys. Res., 100, 24705–24718, 1995.

Pugh, D. T.: Tides, Surges and Mean Sea-Level. Wiley-Blackwell, 1987.

Ray, R. D.: Decadal Climate Variability: Is There a Tidal Connection? J. Climate, 20, 3542–3560, 2007.

250 St. Laurent, L. C., Simmons, H. L. and Jayne, S. R.: Estimating tidally driven mixing in the deep ocean, Geophys. Res. Lett.,
29, 2106, doi:10.1029/2002GL015633, 2002.

Santer, B. D., Bonfils, C., Painter, J. F., Zelinka, M. D., Mears, C., Solomon, S., Schmidt, G. A., Fyfe, J. C., Cole, J. N. S.,
Nazarenko, L., Taylor, K. E., and Wentz, F. J.: Volcanic contribution to decadal changes in tropospheric temperature, Nature
Geos., 7, 185-189, 2014.

255 Solomon, S., Rosenlof, K. H., Portmann, R. W., Daniel, J. S., Davis, S. M., Sanford, T. and J.: Plattner, G-K. Contributions
of Stratospheric Water Vapor to Decadal Changes in the Rate of Global Warming, Science, 327, 1219-1223, 2010.

Stroeve, J. C., Kattsov, V., Barrett, A., Serreze, M., Pavlova, T., Holland, M. and Meier, W. N.: Trends in Arctic sea ice
extent from CMIP5, CMIP3 and observations Geophys. Res. Lett., 39, L16502, 2012.

Tanaka, Y., Yasuda, I., Hasumi, H., Tatebe, H. and Osafune, S.: Effects of the 18.6-yr Modulation of Tidal Mixing on the
260 North Pacific, J. Climate, 25, 7625-7640, 2012.

Webb, D.J.: An ocean model code for array processor computers, Comput. Geosci., 22, 569–578, 1996.

Yasuda, I.: Impact of the astronomical lunar 18.6-yr tidal cycle on El-Niño and Southern Oscillation. Sci Rep, 8, 15206,
2018.

Yasuda, I., Osafune, S., Tatebe, H.: Possible explanation linking 18.6-year period nodal tidal cycle with bi-decadal variations
265 of ocean and climate in the North Pacific, Geophys. Res. Lett., 33, L08606, doi:10.1029/2005GL025237, 2006.

Yndestad, H.: The influence of the lunar nodal cycle on Arctic climate, Journal of Marine Science, 63, 401-420, 2006.

Figure Legends

Figure 1. Top panel- variation in time of the modulation (with reference year for illustrative purposes on the top axis). The tidal modulation f(x,y,t) in the model is the top panel f'(x,y) multiplied by the bottom panel f'(t), multiplied by 1.0 for run

270   CONSTANT, and a scaled function in run SCALED. Bottom panel- geographical distribution of the modulation of tidally-driven diffusivity by the 18.6 year lunar nodal cycle.

Figure 2. Top panel- globally averaged variation with phase of temperature anomalies vs ocean depth (K) vs tidal modulation phase in the SCALED run. Bottom panel- as top panel but for CONSTANT run.

Figure 3: Top panel- variation in time of the modulation. Middle panel – globally averaged ocean heat content anomaly (10^{22}

275   J) vs tidal modulation phase. Bottom panel- globally averaged surface ocean heat flux anomaly (W m^{-2}) vs tidal modulation phase. The mean +/- 2 standard errors are shown for CONSTANT in thin blue, and for SCALED in thin red; sinusoidal best fit curves of global temperature anomalies constructed from all 380 years of analysed output are shown for CONSTANT in thick blue, and for SCALED in thick red; the mean +/- 2 standard errors for 380 years of the control integration of FORTE2 is shown for reference in in black.

280   Figure 4. As Figure 2 but Middle panel- globally averaged surface temperature vs tidal modulation phase. Bottom panel- as for middle panel but for surface temperature in the Arctic region (70°N-90°N).

Figure 5. Top panel- geographical variation in amplitude of sinusoidal trigonometrical fit to surface temperature (K) in SCALED; grey shaded areas show where amplitude is less than 2 standard errors in the CONTROL integration; note nonlinear contour interval. Bottom panel- as top panel but for CONSTANT.

285   Figure 6. Top panel- geographical variation in phase of sinusoidal trigonometrical fit to surface temperature (K) in SCALED. The value is the phase at which the fitted temperature reaches a minimum in terms of the year in the cycle; grey shaded areas show where amplitude is less than 2 standard errors in the CONTROL integration; Bottom panel- as top panel but for CONSTANT.

Figure 7. As Figure 5 but for November-March (NDJFM) mean sea level pressure anomaly (hPa).

290   Figure 8. As Figure 6 but for November-March (NDJFM) mean sea level pressure anomaly (hPa).

Figure 9. Histogram of decadally averaged surface temperature anomalies (K) in CONTROL (black), SCALED (red) and CONSTANT (blue)

Figure 10. Top panel: IPCC AR6 assessed trends for different shared socioeconomic pathways (SSPs). Bottom panel: as top panel but with a lunar nodal cycle of 0.04K amplitude, chosen to be approximately an average of the CONSTANT and

295   SCALED runs.

300
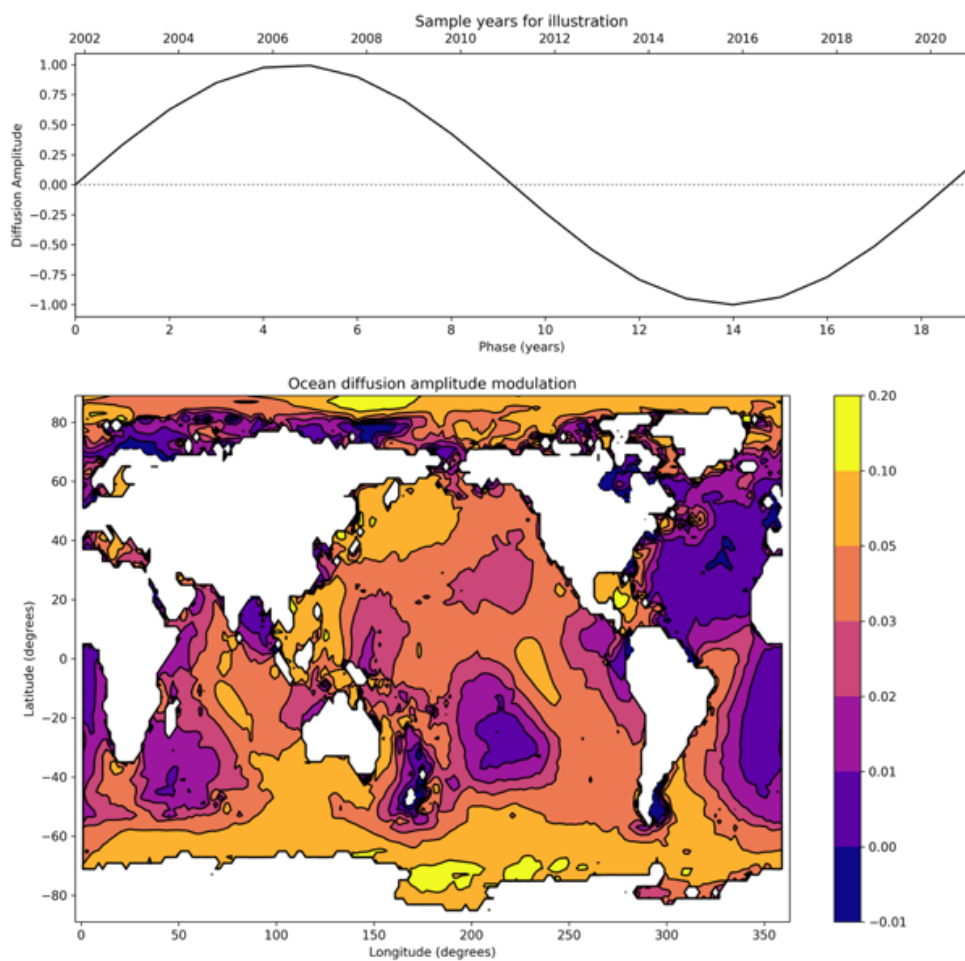
Figure 1
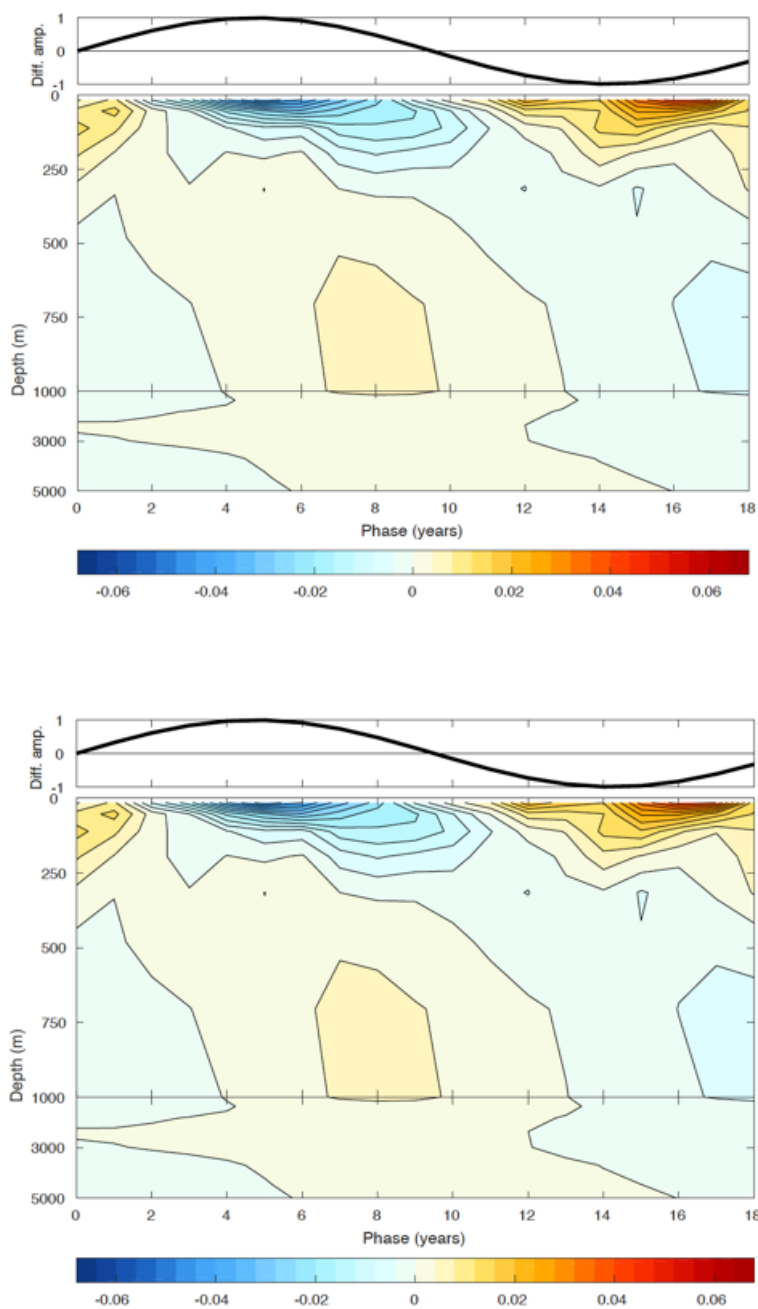
305

Figure 2
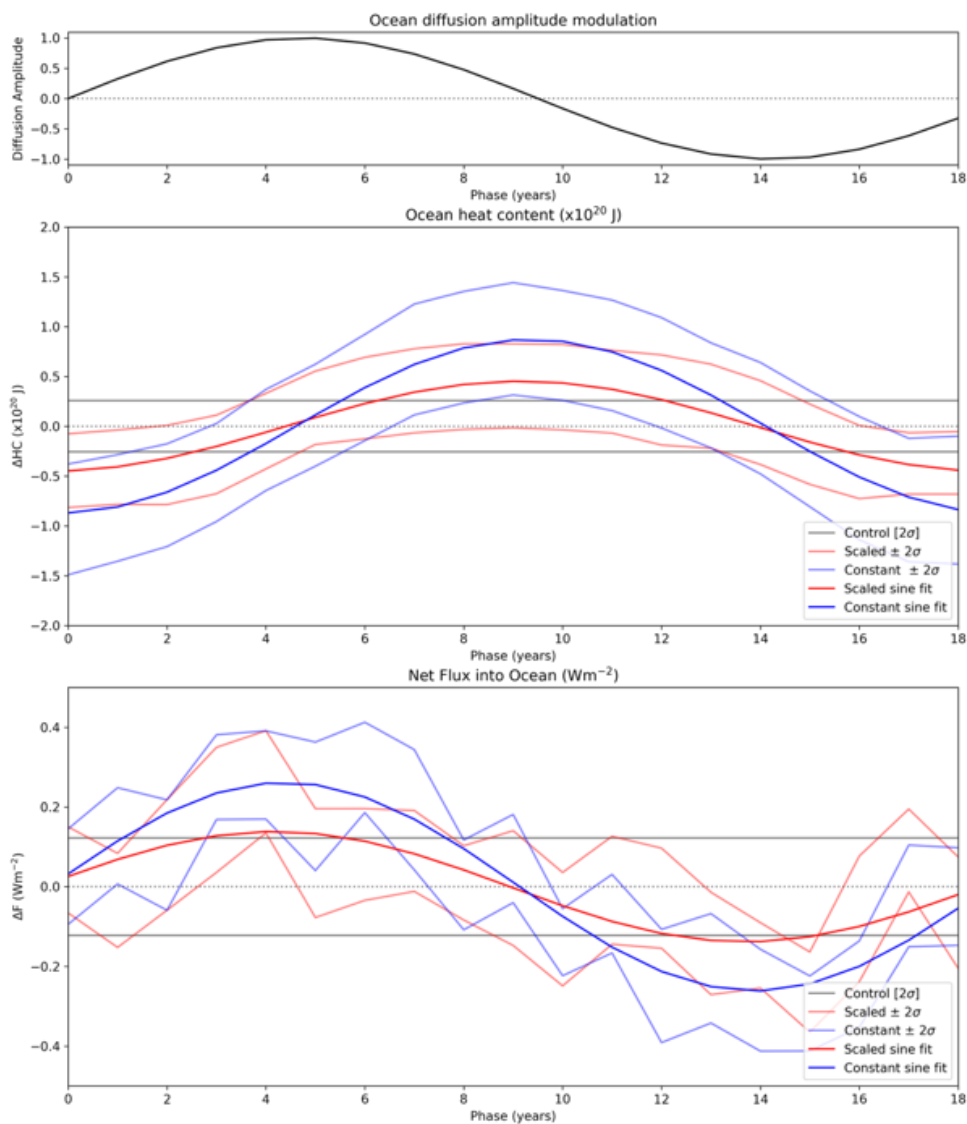
310   **Figure 3**
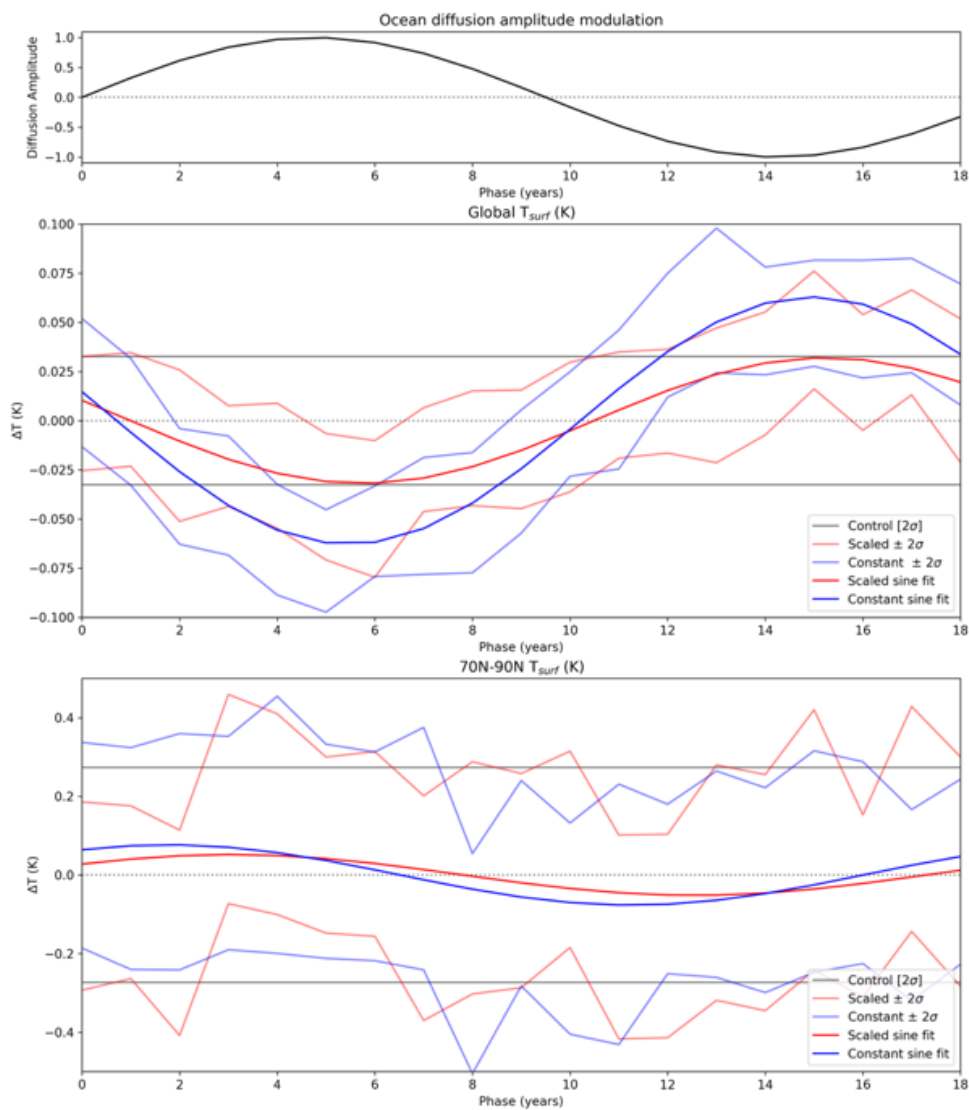
Figure 4
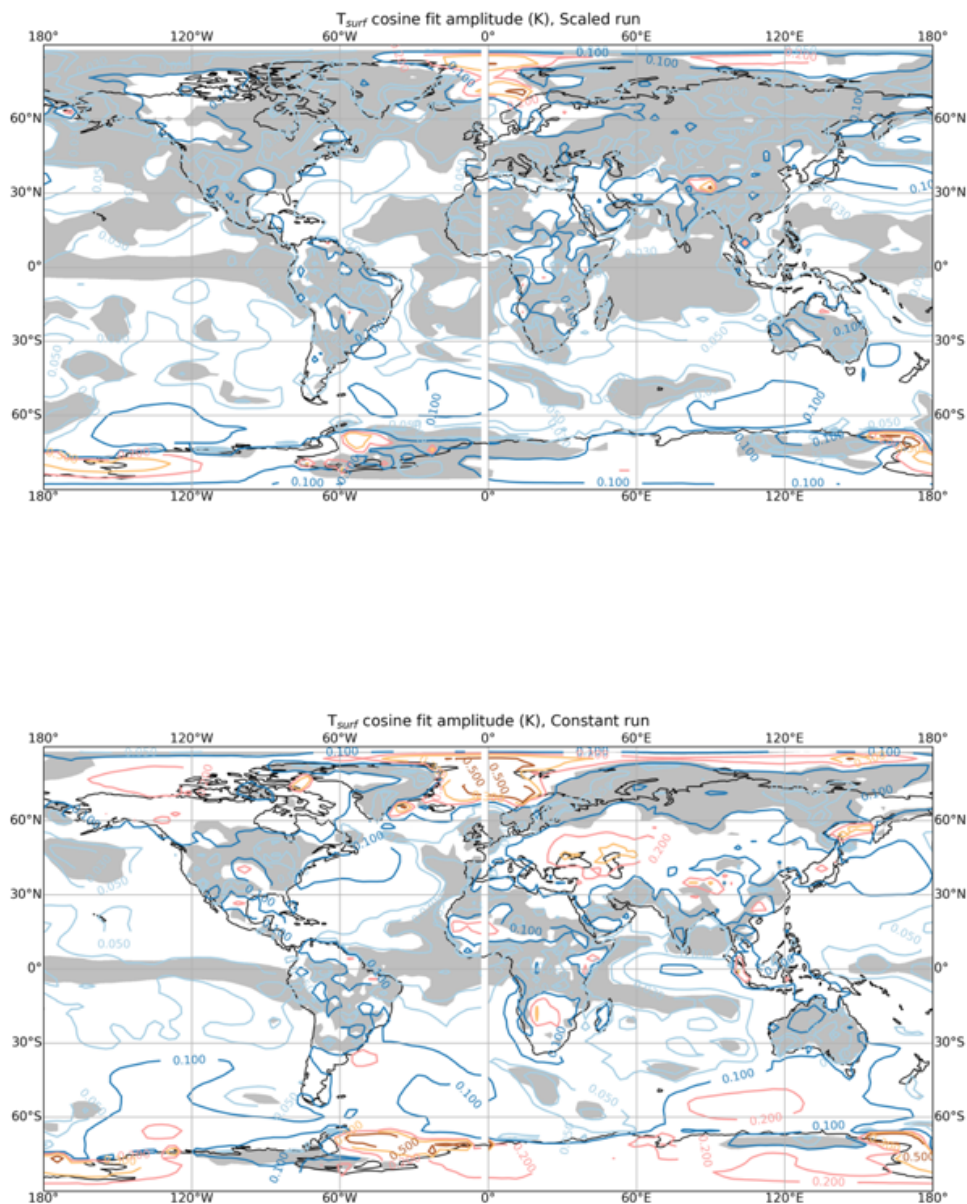
Figure 5
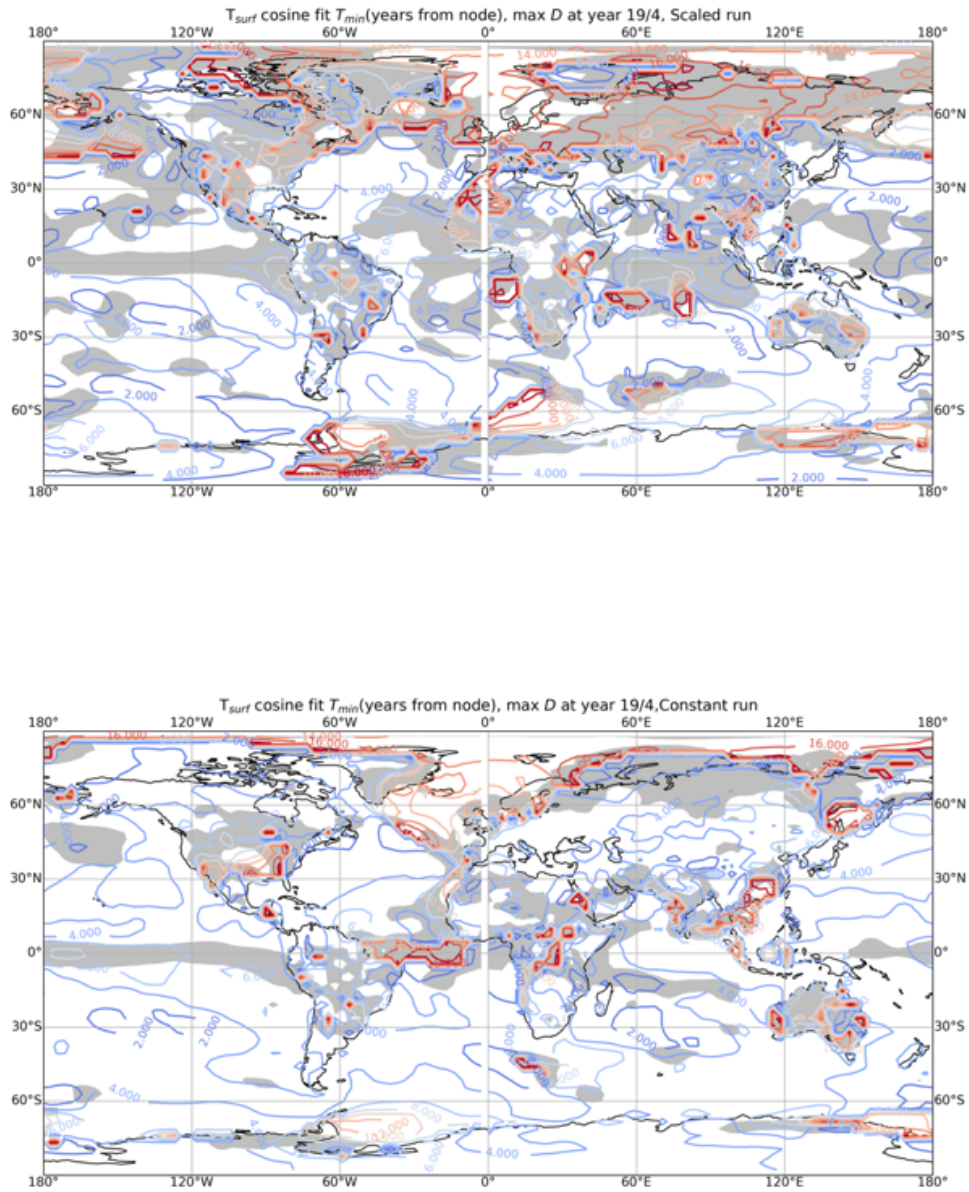
320

Figure 6
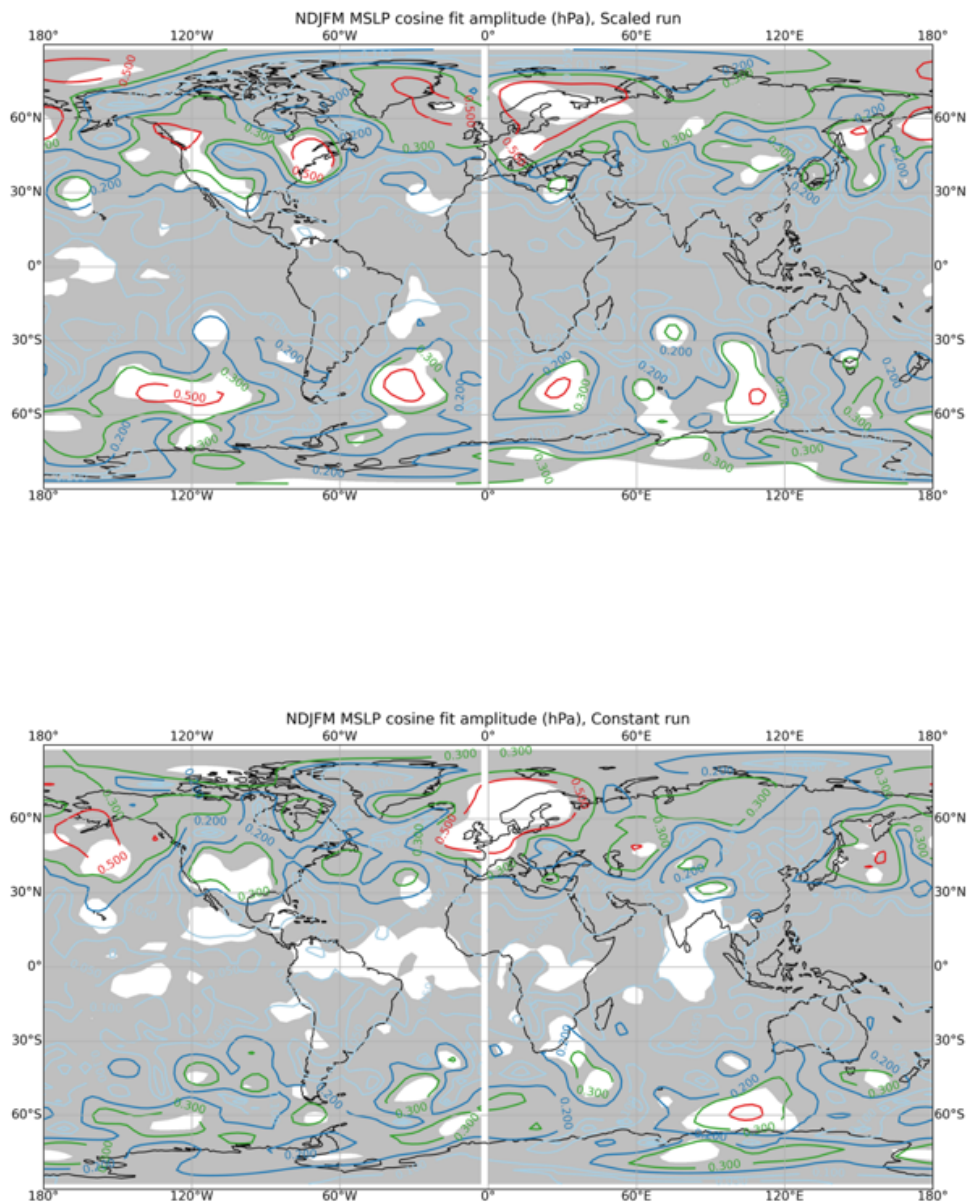
325

Figure 7
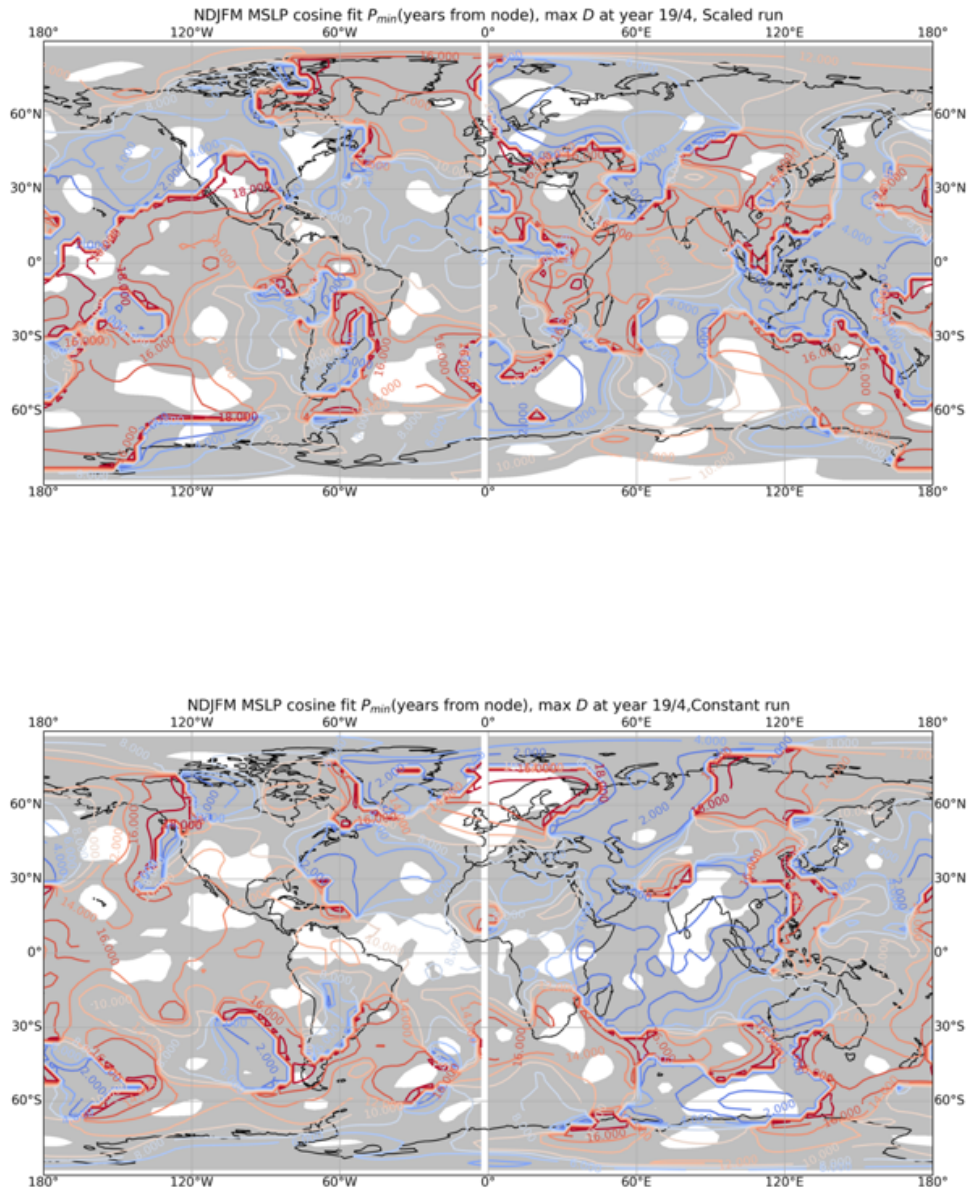
330   **Figure 8**

335   **Figure 9**

Figure 10